EUROFUSION WPMST1-PR(16) 14737

G Meisl et al.

Nitrogen migration in ASDEX Upgrade and JET: Understanding the dependence on surface temperature, roughness and N transport in the SOL

Preprint of Paper to be submitted for publication in
22nd International Conference on Plasma Surface Interactions
in Controlled Fusion Devices (22nd PSI)

This work has been carried out within the framework of the EUROfusion Consortium and has received funding from the Euratom research and training programme 2014-2018 under grant agreement No 633053. The views and opinions expressed herein do not necessarily reflect those of the European Commission.

Nitrogen transport in ASDEX Upgrade: Role of surface roughness and transport to the main wall

G. Meisl[a,*], M. Oberkofler[a], A. Hakola[c], K. Krieger[a], K. Schmid[a], S.W. Lisgo[b], M. Mayer[a], A. Lahtinen[c], A. Drenik[a], S. Potzel[a], L. Aho-Mantila[c], ASDEX Upgrade Team[a], the EUROfusion MST1 Team

[a] *Max-Planck-Institut für Plasmaphysik, Boltzmannstraße 2, 85748 Garching, Germany*
[b] *ITER Organization, FST, Route de Vinon, CS 90 046, 13067 Saint Paul Lez Durance Cedex, France*
[c] *VTT Technical Research Centre of Finland, P.O.Box 1000, FI-02044 VTT, Finland*

Abstract

We have studied the retention of nitrogen in surfaces with varying roughness and the transport of nitrogen from the divertor to the outer midplane in experiments at the tokamak ASDEX Upgrade. To allow for a reliable identification of nitrogen retained from the plasma exposure, $5.3 \cdot 10^{21}$ atoms of the tracer isotope ^{15}N were injected into the private flux region of the plasma. On polished W samples exposed to the plasma in the outer divertor, the N content peaks to both sides of the strike line with an areal density of $1.5 \cdot 10^{20}$ ^{15}N/m^2 and drops to a value of $1.0 \cdot 10^{20}$ ^{15}N/m^2 in the strike line region. In contrast, the N content of samples with a rougher surface peaks at the strike line and reaches areal densities of $3.0 \cdot 10^{20}$ ^{15}N/m^2. The N deposition at the outer limiters was measured via samples exposed on the midplane manipulator. At the limiter position the ^{15}N areal density reaches a value of $0.2 \cdot 10^{20}$ ^{15}N/m^2, only a factor of ten smaller than the areal densities in the divertor. However, a comparison to WallDYN simulations shows

*Corresponding author address: Boltzmannstr. 2, 85748 Garching, Deutschland
Email address: gmeisl@ipp.mpg.de (**G. Meisl**)

that the observed N content is roughly a factor of 4 smaller than the value predicted by these simulations. Possible reasons for this discrepancy are the toroidal asymmetric main wall geometry, which currently cannot be fully included in the simulations, or an enhanced re-erosion of deposited N.

Keywords: *PACS:* 52.25.Vy, 52.40.Hf, 52.52.Fi, 52.55.Fa

---

1. Introduction

The migration of impurities is a key process in the area of plasma-surface interaction because it controls material erosion and mixing and plays an important role in the tritium retention [1]. Resulting from the successful application of nitrogen for radiative cooling in tokamaks with W or W/Be surfaces [2], questions related to the plasma-wall interaction of N appeared. While nitrogen is chemically inert in the gaseous phase (N_2) it can form chemically highly reactive radicals in the plasma. Of special concern are the wall pumping effect [3], the temperature stability of nitrides formed by N ion implantation [4, 5], the ammonia formation [6, 7], the deuterium fuel retention in surfaces with N [8] and erosion of WN [9].

This paper focuses on two special aspects of the N migration in tokamaks, the impact of the surface roughness on N retention in W surfaces and the transport of N from the divertor, where it is typically puffed, to the main wall. The need to understand the role of surface roughness originates from the prevalence of (technically) rough surfaces in fusion plasma experiments, while well-defined polished surfaces are employed in laboratory experiments. Roughness could be expected to play an especially important role for N retention, because N is only stored in the implantation zone of a surface and the N content saturates at areal densities of about $1.0 \cdot 10^{20}$ $^{15}\mathrm{N/m^2}$, corresponding to a 3 nm thick WN layer [4]. On a rough surface the effective surface area (and the resulting effective saturation areal density) may be significantly larger than the geometric surface area.

The transport of N to the main wall is of importance for several reasons: First, a

strong contribution of the main wall to the N retention in the ASDEX Upgrade (AUG) vessel was suggested to bring together the N saturation observed in direct measurements of the N areal density and the amount of N retained in the AUG vessel from balance estimations [10]. Furthermore, WallDYN simulations of N migration indicate that the N concentration in the core plasma increases when pumping of N by the main wall decreases with increasing level of saturation [11]. Secondly, W sputtering of plasma exposed surfaces is mostly governed by the flux of impurities like N on such surfaces. Therefore, the N fluxes to the main wall are an important input for estimating the main wall erosion. Finally, an important question related to the ammonia formation is identifying the surfaces where ammonia is produced. As the N influx is expected to be one of the major quantities determining the ammonia formation, the N flux to the main wall is required for estimating the ammonia production in this region.

2. Experimental set-up

Studies of N transport and WN_x formation in tokamaks are hindered by the inevitable presence of a ^{14}N background from air. In contrast, the injection of ^{15}N, with an abundance of only 0.37 % in atmospheric N_2, permits an essentially background free determination of the N deposition from the plasma exposure and has already been successfully tested in Ref. [12]. In this experiment, a total of $5.3 \cdot 10^{21}$ ^{15}N atoms were injected into low power deuterium plasma discharges at AUG (shot numbers #32019–32024). To maintain toroidal symmetry, valves with 4 toroidally distributed outlets in the roof baffle were chosen for the $^{15}N_2$ puff (see Fig. 1). This choice is also of practical relevance, as these valves are regularly used for N_2 injection at AUG. As can be seen in Fig. 2, an average

N_2 puff of $2.9 \cdot 10^{20}$ N/s was chosen. As a minimum flux is required to open the valves, a modulation of the puff (10 ms on, 30 ms off) was required. The valve is connected to the outlets in the roof baffle via a 3 m long tube. The time required for the N_2 to move from the valve location through the tube to the outlet is above 0.1 s, so that the original modulation in the puff is smoothed out.

The well diagnosed L-mode discharge from Ref. [10] was chosen as reference scenario, with moderate ECRH heating of about 400 kW and a line averaged density of $4 \cdot 10^{19}$ m^{-3}. To provide a source of neutral particles for measurements of the core N concentration with charge exchange recombination spectroscopy (CXRS), short blips with the NBI heating system were required. Probably due to variations in the machine conditions, the aspired L-mode plasma was only reached in part of the discharges, while especially the first discharges were in the I-phase, an intermediate state between L-mode and H-mode [13, 14]. As can be seen from the electron temperature measurement in Fig. 2, the I-phase plasma resulted in fluctuating SOL plasma conditions.

The magnetic geometry and the position of the exposed samples are shown in Fig. 1. The recently installed divertor manipulator system (DIM-II) allows to expose several poloidal rows of samples under similar conditions at the same toroidal position [15]. In this experiment we exposed four sets of samples:

- Bulk W samples mechanically polished to a mirror like surface finish.
- W coated fine grain graphite samples, where the substrate was mechanically polished and coated with a tungsten layer of 100–120 nm thickness. The polishing procedure resulted in a mostly smooth surface with holes of about 1 μm in size.

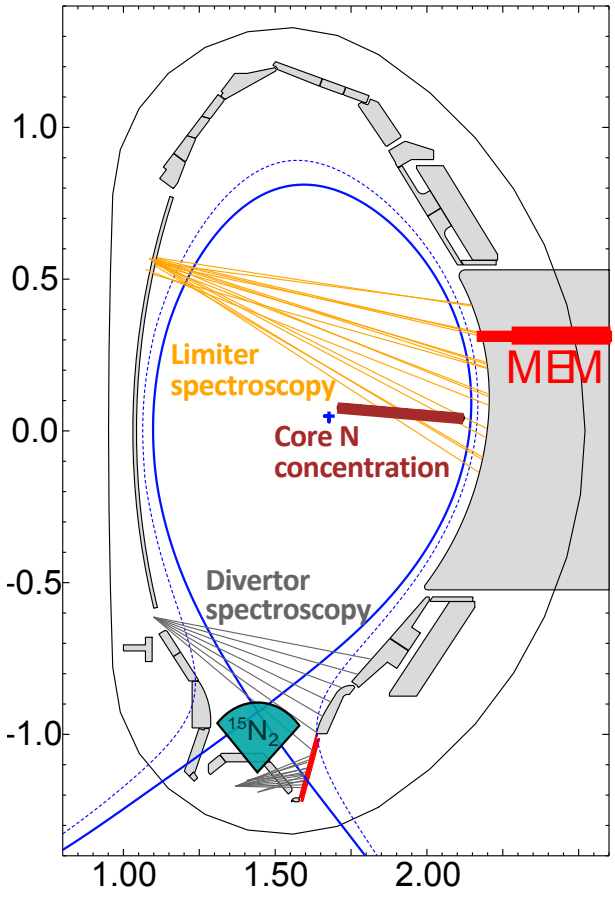

Figure 1: Geometric setup of AUG experiments with the $^{15}N_2$ puff into the private flux region, the location of the deposition probes at the outer divertor and outer midplane and spectroscopic lines of sight. The flux surface hitting the uppermost divertor sample is about 2 cm away from tip of the Midplane Manipulator (MEM).

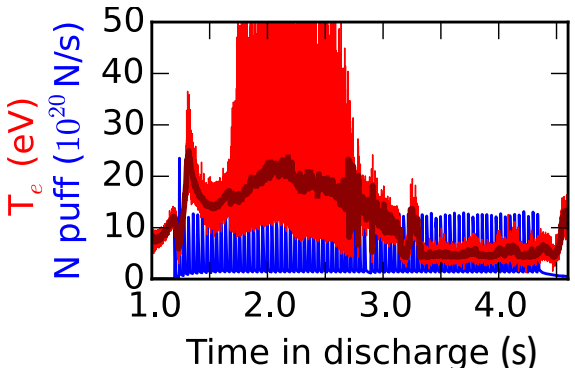

Figure 2: N_2 puff (blue curve) and T_e from a Langmuir probe close to the outer strike line during discharge #32024 (red curve and time averaged dark red curve). During I-phase the electron temperature at the outer strike line exhibits strong fluctuations.

- W coated fine grain graphite samples, where the graphite surface remained in its milled state and was coated with a tungsten layer of about 120 nm thickness. These samples had, similarly to the samples employed in Ref. [16], a rather rough surface consisting of structures in the range from 10–100 μm.

- Bulk Mo samples mechanically polished to a mirror like surface finish.

Scanning electron microscope images (SEM) of the bulk W and W coated samples are shown in Fig. 3. Each set consists of six samples which, with a total poloidal length of 20.1 cm, give a comprehensive coverage of the outer divertor target plate.

The deposition of N at the low field side (LFS) midplane was studied by exposing a cylindrical graphite cylinder coated with a W layer of several micrometer thickness by combined magnetron sputtering and ion implantation [17] to the plasma with the midplane manipulator system (MEM). The cylinder had a total length of 8.9 cm and was kept at a constant position with its tip about 2.5 cm ahead of the ICRH limiters for the six consecutive discharges. Because of a very short contact of the plasma with the sample in

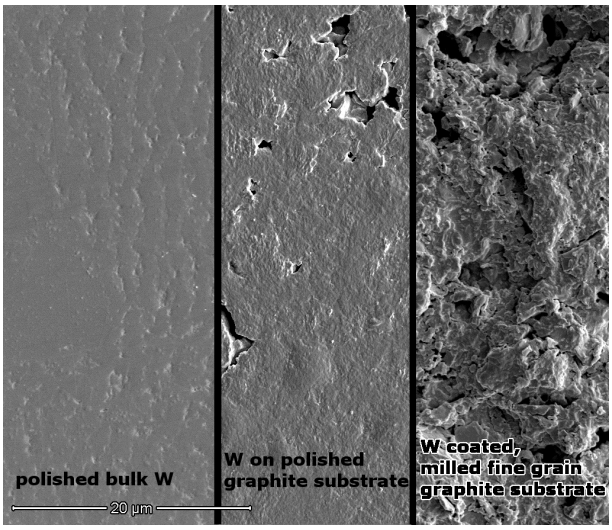

Figure 3: SEM images of a polished bulk W sample, a W coated polished graphite sample and an unpolished W coated graphite sample after plasma exposure. The bulk W sample has a flat surface, the polished graphite substrate is largely flat but has some micrometer-sized holes and the unpolished surface is very rough.

the ramp up phase, the sample surface heated up to a peak temperature of about 800 K. After the intense contact the sample cooled down to below 500 K within 0.3 s.

A three dimensional CAD drawing which shows the position of the MEM relative to the neighboring auxiliary limiters is shown in Fig. 4. The magnetic field in the MEM region is rather horizontal and the distances to the nearby and distant auxiliary limiters are 0.3 m and 1.5 m, respectively.

To determine the amount of ^{15}N on the samples after exposure to the plasma, we used nuclear reaction analysis (NRA). The α particles resulting from the reaction ^{15}N (^{1}H, ^{4}He) ^{12}C were counted at a reaction angle of 135°. The number of counts resulting from irradiation with 1 MeV protons was converted into the N areal density by the cross section given in Ref. [18]. Also particles emerging from nuclear reactions of the protons with boron [19] were recorded and quantified by comparison to a calibration sample with known boron

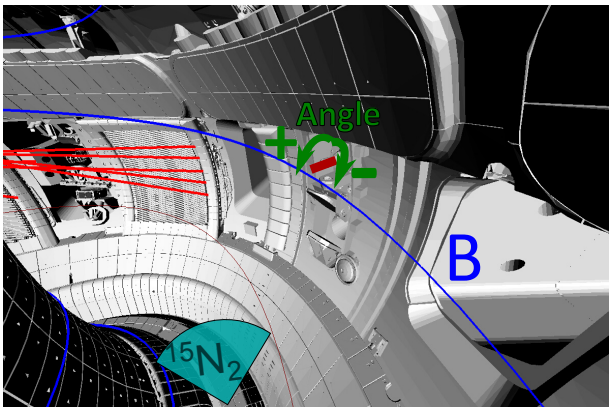

Figure 4: CAD drawing of the AUG vessel showing the position of the sample exposed at the low field side (LFS) midplane, a magnetic field line passing at the tip of the sample and some of the spectroscopic lines of sight observing the ICRH limiters. Positive angles in Fig. 8 indicate measurements on the back of the sample (facing the nearby auxiliary limiter).

content. The detector had a solid angle of 22 ± 1 msr and was covered with a Mylar stopper foil having a thickness of 18 μm. The beam spot was 1x1 mm^2 on the target at normal incidence. To determine the deposition of carbon, which might lead to co-deposition of N, and of ^{14}N from the residual gas, which might compete with the ^{15}N[1], some of the samples were also analyzed by NRA with ^{3}He (utilizing the $^{12}\mathrm{C}\,(^3\mathrm{He}, p_x)\,^{14}\mathrm{N}$ and the $^{14}\mathrm{N}\,(^3\mathrm{He}, p_x)\,^{16}\mathrm{O}$ reactions) and ^{4}He (utilizing the $^{14}\mathrm{N}\,(^4\mathrm{He}, ^1\mathrm{H})\,^{17}\mathrm{O}$ reaction) projectiles. The number of protons emerging from these reactions were converted to areal densities by comparison to calibration samples.

[1]If a surface is already saturated with ^{14}N, isotope-exchange processes would be required to store additional ^{15}N atoms.

3. WallDYN modeling of N transport and retention

Especially for the transport of impurities over longer distances, not only the direct transport path, but also multi step transport processes might play a role. To study the transport including the effect of such multi step processes WallDYN simulations of the present experiment have been performed [20, 21]. This model simulates the time evolution of the surface composition of the first wall, which is discretised for this purpose into 59 poloidally distributed wall tiles.

An important input to the WallDYN simulations, which provides basic information for the simulation like the plasma density, temperature and flow pattern and the fluxes of deuterium atoms and ions to the walls is the plasma background. Based on the plasma background a set of DIVIMP [22] simulations is used to parametrize the impurity transport through the plasma and finally WallDYN combines the information on the deuterium fluxes, the impurity transport and models on the plasma-wall interaction to calculate the evolution of the impurity fluxes and the surface composition [20]. To check the sensitivity of the WallDYN simulations with respect to the plasma parameters, three different plasma backgrounds have been employed for the present work:

- The non-seeded and the N-seeded SOLPS plasma backgrounds extended to the far SOL with an onion-skin model (OSM) described in Refs. [16, 10].

- A plasma background employing the N-seeded SOLPS solution in the divertor region and an OSM solution based on this SOLPS background but featuring a slightly different flow pattern of the upstream plasma [23]. The flow pattern was chosen as parameter to be modified because it is not reliably reproduced in SOLPS solutions

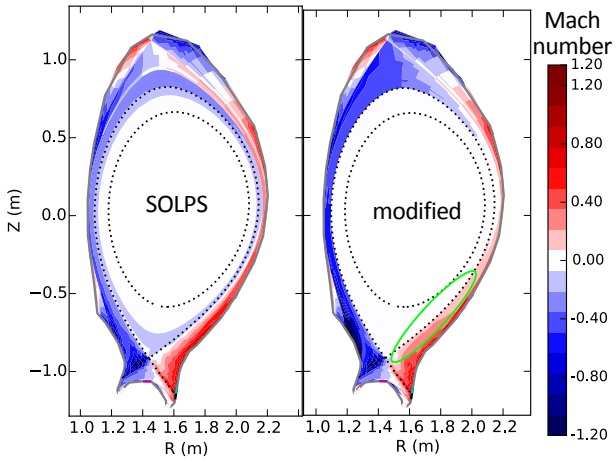

Figure 5: D^+ flow patterns of the N-seeded SOLPS background and a background where the upstream SOL flow pattern was modified to feature stronger flows to the HFS divertor and a flow directed to the outer divertor below the outer midplane (marked by the green circle). Positive flows are directed towards the outer divertor.

but known to have a strong impact on the impurity transport in the plasma [24]. A graph with the flow profiles for the N-seeded SOLPS plasma background and this plasma background with modified flow profiles is shown in Fig. 5.

The transport of particles perpendicular to the magnetic field lines can be modeled in DIVIMP by a combination of anomalous diffusion and convection. The reference simulation employed a diffusion coefficient of $D_\perp = 0.5\ m^2s^{-1}$, the value of the particle diffusion coefficient used in the SOLPS simulation of the background plasma close to the separatrix. As described later, simulations with higher diffusion coefficient or an additional convective outward transport velocity in the far SOL were performed with the aim to improve the agreement with the experimental results. Based on the conclusions from Ref. [10], N atoms are launched as atoms with an energy of about 0.03 eV.

To account for the limited N storage capacity of W surfaces in the WallDYN simu-

lations, the N concentration in the reaction zone was limited as described in Ref. [10]. In net-deposition areas where N is co-deposited with B or W, the N areal density may still rise to values above this saturation areal density of just under $1 \cdot 10^{20}$ N/m^2. Due to regular boronisations, parts of the AUG first wall are covered with boron. The initial wall composition in the simulations was pure tungsten around the outer strike point and a mix of 40 % tungsten and 60 % boron for the rest of the wall. Boron, like tungsten, forms stable compounds with N, so the same N saturation model is applied for boron containing regions of the wall. To mimic the pumping of N_2 by the vacuum system, sputter and reflection yields in the respective areas of the divertor were set to zero as described in Ref. [16]. Pumping by diagnostic systems in the main chamber is not included in this model.

Modelling of flux enhancement on main wall limiter structures. As can be seen in Fig. 4, the LFS main wall area is not toroidally symmetric, but consists of limiter structures close to the plasma and recessed areas. To include this structure to a first order in the 2D WallDYN simulations, the so called "recessed area" model is employed. This model introduces additional wall tiles so that both the limiters and the recessed wall areas are adequately described. The fraction of the wall which is attributed to the limiters and the fraction attributed to the recessed areas are specified by the user. For this work the limiters were estimated to represent twenty percent of the low field side main wall. The particle fluxes and ion energies for these wall tiles are calculated based on the following assumptions:

- The ratio of the main ion species (taken from the plasma background) and impurity

fluxes to the front and recessed surfaces are calculated from user specified values for the decay length (3 cm for this work) and the distance between the front and recessed surfaces (15 cm for this work). This leads to an increase of the fluxes to the front surfaces in comparison to simulations assuming a toroidally symmetric wall.

- The electron and ion temperature of the plasma at the recessed areas, which is required to calculate the impact energy of the ions, is evaluated from a user specified decay length and the distance between the front and recessed surfaces.

- The fluxes and energies of charge-exchange neutral fuel particles are identical for front surfaces (limiters) and recessed surfaces.

- The transport of impurities starting from the front or recessed areas is not changed by the toroidal asymmetry.

Previous simulations have shown that this model mostly results only in small changes for the global erosion/deposition patterns[2]. For the N transport, however, the toroidal asymmetry leads to a faster saturation of the N content in the front areas and thereby to a different time evolution of the N flux at the LFS wall.

Calculation of the radial deposition profile. The analysis of the sample exposed at the outer midplane yields not only one value for ^{15}N deposition at this poloidal position but its radial variation over a distance of several centimeters. Because of its three dimensional nature, this information cannot be extracted directly from the WallDYN/DIVIMP sim-

[2]Of course the local erosion/deposition pattern varies strongly between front and recessed areas, but the total amount of material eroded is comparable.

ulations. To get an estimate for the radial variation from the simulations the following procedure was implemented:

1. The N density in the plasma volume is calculated from the WallDYN/DIVIMP simulations.
2. The radial profiles of the N density (n_N) and D ion temperature (T_i) are extracted at the poloidal position of the MEM.
3. The parallel N flux at this position is estimated from the background ion temperature as $\Gamma_N = n_N \cdot \sqrt{k_B\, T_i / (2\pi\, m_N)}$ where m_N is the mass of the N atoms.
4. An exponential decay is fitted to Γ_N in the region where the sample was exposed, i.e. in the range of 3.5–6.5 cm from the separatrix.
5. An estimate for the N deposition is calculated by integrating the fluxes over time and allowing for an effective reflection/re-erosion fraction of 0.25 as suggested by SDTrimSP simulations.

It should be noted that this procedure is only a very simple approximation for the full, three dimensional model. Though it should give an idea on the decay length, especially the absolute N deposition may be subject to considerable uncertainties.

4. N deposition in the outer divertor

Figure 6 shows the ^{15}N deposition measured on the samples exposed to the outer divertor plasma. The ^{15}N areal density on the bulk W samples reaches its maximum value of $1.5 \cdot 10^{20}$ N/m^2 about 3 cm below and 2 cm above the strike line. From these maxima the ^{15}N areal density decreases towards a value of $1 \cdot 10^{20}$ N/m^2 at the strike line

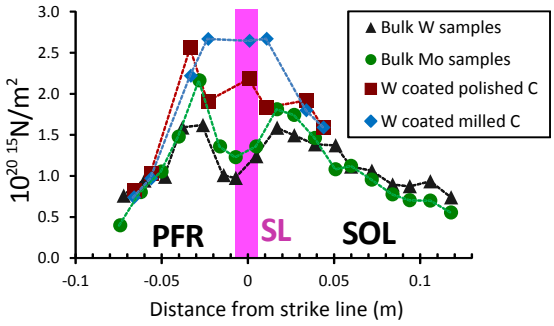

Figure 6: ^{15}N deposition measured on the samples exposed to the outer divertor plasma (circles). The ^{15}N deposition on the bulk samples hovers around $1 \cdot 10^{20}$ ^{15}N/m^2. The ^{15}N content of the W coated C samples is higher close to the strike line and approaches the value of the bulk samples with increasing distance.

and towards values of $0.7 \cdot 10^{20}$ ^{15}N/m^2 at the upper and lower edge of the divertor tile. The ^{15}N deposition profile on the molybdenum sample is similar to that on W, but shows a somewhat larger variation.

A different deposition profile with a peak in the ^{15}N areal densities at the strike line occurs on the W coated graphite samples. The ^{15}N content is comparable to that of the bulk samples in the private flux region and the SOL. In contrast, it does not drop towards the strike line, but goes up to values of $2.5 \cdot 10^{20}$ ^{15}N/m^2. The ^{14}N areal density on the bulk samples is clearly smaller than the ^{15}N areal density and varies in the range of 0.1–0.4$\cdot 10^{20}$ ^{14}N/m^2. A comparison of the ^{15}N data points in the region of 3–5 cm above the strike line to the ^{14}N deposition measurements from [16] shows that the N content after exposure to 6 discharges is only somewhat higher than after 1 or 2 discharges. Interestingly, the N content in this region increases only weakly with the surface roughness.

To support the analysis of the ^{15}N deposition profile and its dependence on the surface

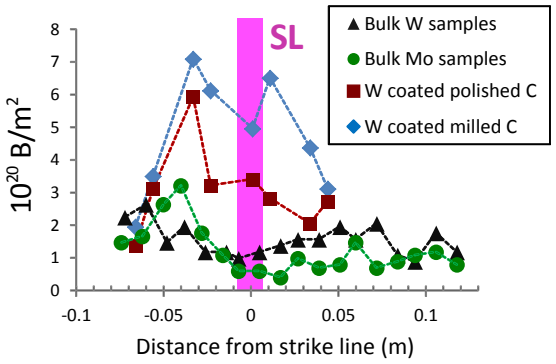

Figure 7: B deposition on the samples exposed to the outer divertor plasma. Around the strike line the B areal density on the rougher samples is much higher than on the well polished bulk samples.

roughness, also the deposition of boron derived from nuclear reactions with the protons used for the ^{15}N measurement is shown in Fig. 7. One can see that the deposition profiles show very similar patterns: The boron areal density on the bulk samples is lower and exhibits a minimum in the strike line region, while the rough samples exhibit a comparatively high B areal density around the strike line. The carbon areal density, which could only be measured on the bulk samples, is comparable to that of boron. A possible explanation for the observed deposition pattern is that for the bulk samples the minimum in the deposition profile around the strike line is caused by a more efficient re-erosion due to higher ion energies. As discussed in Ref. [25], the net erosion rate decreases with increasing roughness, so that the B net deposition rate is higher on the rougher samples. Such a process also is a conceivable explanation for the ^{15}N deposition profiles. However, as discussed above the N content should already be in saturation. Because there are only small differences in the ^{15}N deposition in the region of 3–5 cm above the strike line, the increased effective surface area of rough surfaces apparently does not cause a notable higher saturation areal density. For this reason, a more likely

explanation is the co-deposition of N with boron.

Though a detailed comparison between the measured ^{15}N deposition in the divertor and WallDYN simulations will not be given, it should be noted that the WallDYN simulations shown in Refs. [10, 16] predict a significantly too low N areal density for the region of more than 5 cm above the strike line. This deviation is likely to be related to the overestimation of the N re-erosion discussed in Ref. [10]. A potential explanation for this is the recoil implantation predicted by SDTrimSP [5], calling for a more detailed analysis of N erosion by D in laboratory experiments. Still, it seems also noteworthy that the N flux from the WallDYN-DIVIMP simulations drops significantly faster with increasing distance from the strike line than the N flux in the original SOLPS simulation.

5. N deposition at the midplane

5.1. Experimental results

Figure 8 shows the ^{15}N deposition measured on the samples exposed at the outer midplane. The distance from the separatrix is measured along the axis of the cylinder. The color of the data points gives their angular position θ on the cylinder, where the 0° direction is towards the top of the vessel as indicated in Fig. 4. From the sample tip, where an areal density of $0.7 \cdot 10^{20}$ ^{15}N/m^2 is reached, the ^{15}N deposition decreases to a value of about $0.25 \cdot 10^{20}$ ^{15}N/m^2 at the limiters. Remarkably, on the side of the sample facing the distant limiter (see Fig. 4), the N areal density 2 cm behind the limiter still reaches a value of $0.1 \cdot 10^{20}$ ^{15}N/m^2. The lines give the result from a fit to the data where the free parameters were:

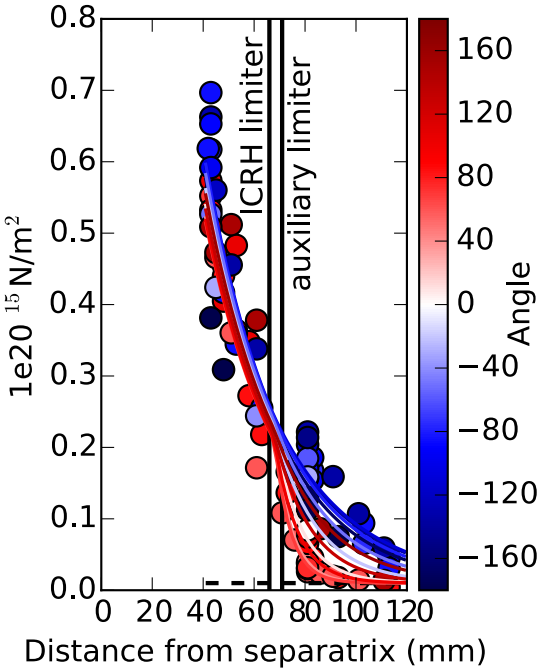

Figure 8: ^{15}N deposition measured on the samples exposed to the plasma at the outer midplane (circles). The color indicates the position on the cylindrical sample, where an angle of 0° points upwards (see Fig. 4). In the limiter shadow the ^{15}N deposition is much stronger on the side facing the distant limiter (blue circles). The lines are fits to the data points.

- A prefactor with an angular dependence (A_1, B_1, Φ_1) for the part of the sample in front of the limiter: $A_1 + B_1 \cos(\theta + \Phi_1)$
- The decay length of the N deposition (without angular dependence) in the part of the sample in front of the limiter represented by an exponential: $\exp(-x/w_1)$
- The decay length of the N deposition in the limiter shadow, including an angular dependence (w_2, w_3, Φ_2): $\exp\left(\frac{-x}{w_2 + w_3 \cos(\theta+\Phi_2)}\right)$

The black dashed line indicates an offset of $0.01 \cdot 10^{20}$ ^{15}N/m^2 attributed to background noise. The decay lengths from this fit are $w_1 = 2.9$ mm in front of the limiter and

$w_2 = 18.6$ mm, $w_3 = 12.5$ mm in the limiter shadow, resulting in decay lengths between 0.6 cm on the sample side facing the nearby limiter and 3 cm for the distant limiter. That means the decay length in the limiter shadow where one could expect a fast parallel loss of the N ions (because the parallel connection length is only of the order of 1.5 m) is similar to the decay length w_1 a few centimeters inside the limiters, where the connection lengths are much larger.

It should be noted that the ratio of the decay lengths in the limiter shadow is very similar to the ratio of the connection lengths, which are about 1.5 m and 0.3 m. Comparing this result to the two models used for modelling anomalous transport (see section 3) leads to the following observation: Estimates for the decay length based on a diffusive model imply a quadratic dependence of the decay length on the connection length [26, equation (6)]. However, with a convective perpendicular transport, the quadratic dependence turns into a linear dependence on the connection length. As this consideration favors the convective description of the perpendicular transport in the far SOL, this description is favored in the WallDYN simulations.

5.2. Comparison of experimental results to WallDYN

A comparison of the measured ^{15}N deposition on the sample exposed to the outer midplane and the corresponding WallDYN predictions is shown in Fig. 9. The gray circles show the experimental data from Fig. 8, while the colored crosses denote the WallDYN results for the N areal density at the poloidal position corresponding to the exposure position. Due to a small difference in the geometry, the wall position in the simulation is at a somewhat larger radius than the actual AUG limiters. The colored

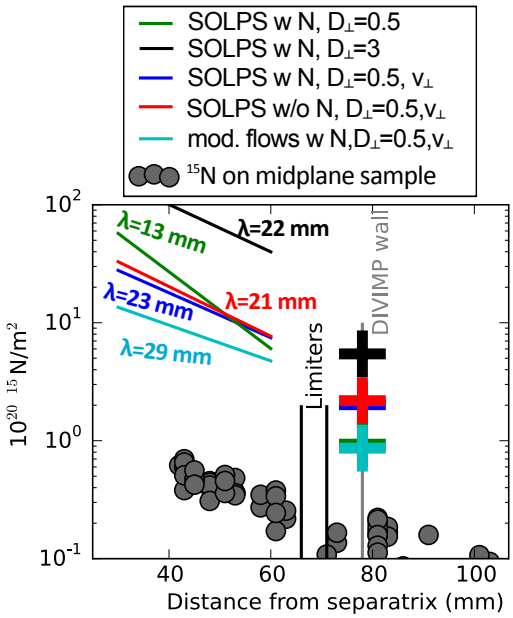

Figure 9: Comparison of ^{15}N deposition predicted by different WallDYN simulations (lines and crosses) and experimentally measured (gray circles).

lines show the radial variation of the N deposition calculated with the model presented in section 3. The lines do not exactly extrapolate to the crosses because the decay length of the simulated fluxes decreases towards the wall.

This comparison shows that the simulations overestimate the N deposition at the outer midplane by about an order of magnitude. Also the predicted radial decay length of the reference case (green curve, based on the N-seeded SOLPS solution) with $D_\perp = 0.5\frac{m^2}{s}$ and $v_\perp = 0\frac{m}{s}$ is significantly too small. Increasing the diffusion transport to $D_\perp = 3\frac{m^2}{s}$ increases the decay length by a factor of two. This results in a better agreement with the experimental value but also in a higher N deposition at the midplane. To somewhat decouple the decay length from the total flux to the wall, a spatially varying perpendicular transport was introduced in the DIVIMP simulations. To this end, based on the analysis of the N transport into the limiter shadow, an outward directed convective transport

velocity of $v_\perp = -40\frac{m}{s}$ was applied for cells which have an upstream distance of 2 cm or more from the separatrix. The perpendicular diffusion was kept fixed at the value of $D_\perp = 0.5\frac{m^2}{s}$. As can be seen in the blue curve, this leads also to a larger decay length of 23 mm with a smaller increase in the predicted N deposition. To test the impact of a hotter divertor plasma on the transport to the midplane, a simulation based on the non-seeded SOLPS solution has been performed (red data). One can see that the predicted decay length and amount of deposited N only change little in comparison to the same simulation with the N-seeded background. This is an indication that the difference in divertor conditions between the I-phase and the L-mode has a modest effect on the transport to the midplane. Finally, the plasma background with the modified SOL flow pattern was used for the calculation of the light blue data. Especially the downward directed flow of the SOL in the LFS X-point region reduces the upstream transport of N and also the decay length increases. Still, the absolute amount of deposited N remains too large.

Problems of the ^{15}N deposition are the integration over a long time period with several individual plasma discharges and processes like re-erosion of previously deposited N, which may hamper the interpretation. In comparison to that, the quantification of spectroscopic measurements is not as reliable due to error sources like the photon emissivities and reflection of light from the metallic walls, but the measurements have a much better time resolution. A comparison of the WallDYN simulations to spectroscopic measurements with lines of sight viewing the LFS wall and divertor is shown in Fig. 10 for the L-mode phase of #32024, for which the plasma backgrounds should be most appropriate. The highest spectroscopic N intensities appear in the divertor. Within the comparatively large

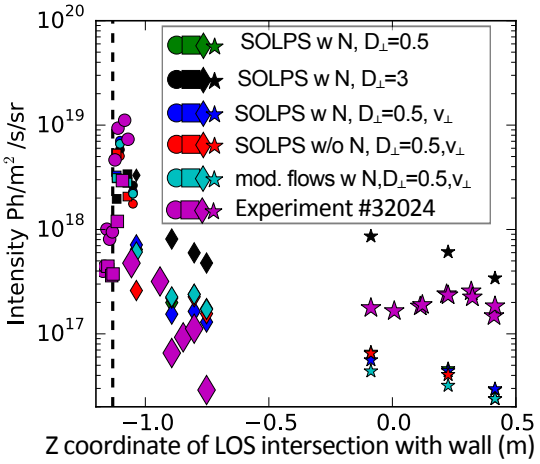

Figure 10: Comparison of WallDYN simulations to N intensities measured (magenta symbols) with spectroscopic lines of sight viewing the LFS wall and divertor. The lines of sight viewing the ICRH limiters lie in the range from Z=-0.15 – 0.5 m.

scatter of signals from lines of sight viewing the same poloidal area in the divertor (■ and ● symbols), the simulations reasonably agree with the measurements. The main difference between the simulation and the measurements in this region is a faster drop of the intensities above the strike line and a much steeper drop towards the private flux region.

Going upwards to the outer baffle (♦ symbols) the difference between the simulations and the experimental measurements, but also the scatter in the experimental measurements, increases. In this region, the experimental intensities are below the simulated ones. In contrast, most of the simulated intensities are again below the measured ones for the lines of sight observing the ICRH limiters (★ symbols). Only the simulation with $D_\perp = 3$ m^2/s produces intensities which are significantly higher than the measured ones. The different spatial profiles of the measured and simulated intensities could be caused by small differences in the magnetic configuration, where the magnetic field lines in the

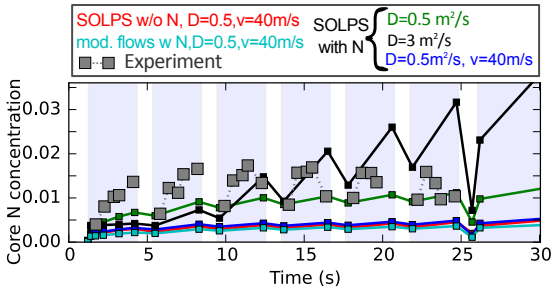

Figure 11: Comparison of core N concentration from WallDYN simulations and discharges #32019–#32024. The phases with N_2 puff are indicated by the light blue background color. The red, light blue and blue curves are based on DIVIMP simulations where an outward directed convective transport was applied in the far SOL. More details on the different simulations are given in the text and previous figures.

simulation partly intersect with the walls while the experimental magnetic field followed the wall shape very closely. Additionally, it should be mentioned that the experimental intensities in the limiter region (Z=-0.15–1.5 m) increase by about a factor of two from the first to the last discharge. The increase in the predicted spectroscopic intensities with time is smaller than the experimentally observed one for the WallDYN simulations with $D_\perp = 0.5$ m^2/s and larger for $D_\perp = 3$ m^2/s.

Finally, the simulations shall be compared to CXRS measurements of the N concentration in the core plasma. Because of the spatial proximity, the N core density is likely to be closely related to the N flux to the main wall. The spatially averaged N core concentration during #32019-24 is shown in Fig. 11 together with the WallDYN predictions. It should be noted that the N concentration during the I-phase peaks in the plasma center. When the plasma switches into the L-mode, also the N density drops as can be seen for example in the range from 22 s to 24 s. Comparing the simulations to the core N concentration during L-mode, the reference case (green) gives a very good agreement. The application of an outward directed convective N transport in the outer SOL, which resulted in the

best agreement between simulation and experiment in Fig. 9, also leads to a reduction of the core N concentration below the experimentally observed value. However, as effects like potential poloidal asymmetries are not included in the DIVIMP simulations, these lower core N concentrations still are considered to be in reasonable agreement with the experimental data. The simulation with $D_\perp = 3$ m^2/s results in reasonable absolute N concentrations, too. However, the strong increase of the N content with time is not observed in the experiment.

Figure 12 shows that on a longer time scale all simulations predict such an increase in the core N content. This rise is caused by an increased N recycling at the main wall surfaces, from where N atoms have a comparatively high probability to enter the core. For reference, Fig. 12 also shows experimental data from a set of nearly identical H-mode discharges with a higher heating power, which allows a higher N injection rate and a longer flat top phase. The measured core N density rises roughly linearly with the number of injected N atoms until about 10^{22} N atoms and rises by another factor of two until it saturates at about $3.5 \cdot 10^{22}$ N atoms. Due to the complex H-mode core transport an agreement in the absolute value of the core N density should not be expected. Still, a higher recycling level at the main walls should increase the N influx into the core plasma and thereby the core N concentration. However, such a strong increase in the core N density as predicted by WallDYN is not observed experimentally.

5.3. Discussion and conclusion

This section showed the first experimental measurements of N transport from the divertor region to the main wall. After injection of $5.3 \cdot 10^{21}$ ^{15}N atoms the N areal

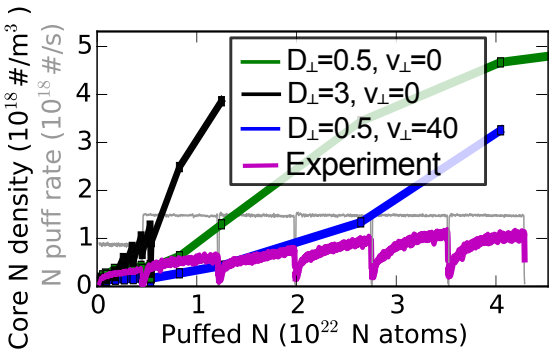

Figure 12: Comparison of the core N density evolution predicted by WallDYN for the discharges #33028–#33033 as a function of the number of injected N atoms for a series of nearly identical H-mode discharges with a N puff rate of $1.5\,10^{21}$ N/s. The simulations predict a strong increase in the core N density after the injection of 0.5–3 10^{22} N atoms.

density at the outer limiters is in the range of 10–30 % of the areal density in the outer divertor. Thereby, the ^{15}N deposition extends several centimeters into the limiter shadow. Because the main wall surface area is considerably larger than the divertor surface area, this results in a significant contribution of the main wall to the total N wall storage. Furthermore, the N content of the main wall is likely to rise faster than the N content in the divertor, which is already in saturation. Qualitatively this agrees well with earlier WallDYN predictions [16].

A detailed comparison between WallDYN simulations and experimental results shows that the areal densities predicted by WallDYN are an order of magnitude higher than the experimental ones. The best agreement between experimental data and simulations is reached with a modified SOL flow pattern and an additional convective outward transport which is only active in the far SOL. Comparisons of the simulations to spectroscopic measurements from the ^{15}N seeded discharges give a reasonably good agreement, but do not show a pattern which would help to understand the discrepancies in the ^{15}N deposition.

Furthermore, the long term evolution of the core N density seems to be different in the simulations and the experiment. This heterogeneity in the experimental and simulation results makes it unlikely that the observed deviations are caused by only one process but indicates that several processes may contribute to the observed discrepancy:

- There are indications that, especially for elevated surface temperatures, the N re-erosion is higher than expected from pure physical sputtering [5, 27]. Furthermore, the core N concentration measurments show that the N content in the beginning of a discharge is lower than at the end of the previous discharge, indicating that the ramp-up and ramp-down phases might contribute to the N re-erosion. Already a comparatively small re-erosion at the sample tip could have profound consequences: As the re-erosion depends on the concentration and probably also the surface temperature at the respective position, the measured deposition would not only be too low but also too flat. For the simulation employing the modified flow profile this means that the perpendicular transport should be reduced, which would in turn reduce the predicted N deposition.

- Processes which are not included in the DIVIMP transport calculations might reduce the transport of N to the midplane. For example, the importance of drift effects on the impurity migration have been observed earlier [28] and in SOLPS simulations drifts decreases the core N concentration [29]. Also the I-phase fluctuations (or ELMs in the H-mode data shown in Fig. 12) or the release of N in form of N_2, as discussed in Ref. [30] or NH_3 molecules could reduce the N content of the upstream plasma.

- Inaccuracies in the main wall geometry or 3D effects, like the transport of reflected neutral N atoms to recessed areas, could lead to a distribution of N on a larger surface area. An increased deposition area would reduce the flux to a specific surface like the exposed sample and reduce the core N density by increased wall pumping. Actually when the recessed wall model is not used in WallDYN, the areal density at the outer midplane agrees nicely with the experimental value.

- Finally, the presence of ^{14}N in the W surfaces prior to the ^{15}N injection could affect the ^{15}N transport and deposition. First, the implantation of ^{14}N into the midplane sample could lead to a reduced ^{15}N capacity of the surface. However, NRA measurements after the exposure show that the ^{14}N areal densities over most of the sample is below $0.2 \cdot 10^{20}$ ^{14}N/m^2 and might be a little bit higher with values of $0.4 \cdot 10^{20}$ ^{14}N/m^2 in the millimeters closest to the plasma. Second, the presence of N in the wall surfaces should reduce the wall pumping and, therefore, increase the (stepwise) transport of ^{15}N to the main wall. Actually, the simulations show that indirect migration paths, mainly via the outer divertor baffle, significantly contribute to the N flux onto the midplane. This would would increase the discrepancy on the N deposition at the outer midplane, but might partly explain the different temporal evolutions observed in Fig. 12.

To summarize, the experimental results confirm the qualitative picture for the N retention in W and its migration in tokamaks. However, quantitatively the experimental results cannot be explained yet. For the tokamak transport simulations this means that further efforts should be made to use 3D transport codes including drifts for the long

range transport of impurities. With regard to the re-erosion of N from tungsten nitride, the presented results indicate an overestimation of the N re-erosion in the divertor with its low surface temperature and an underestimation of the re-erosion from the midplane sample, which reached comparatively high temperatures during the ramp up phase. This result calls for more detailed investigations of re-erosion of tungsten nitride by D, especially its temperature dependence and the N depth distribution under simultaneous D-N bombardment.

The different core N density evolution shown in Fig. 12 might be of special importance for the simulation and application of the power exhaust with N seeding. The ratio of the impurity concentration in the divertor and the concentration in the core plasma is an important figure of merit in such studies. On one hand, the WallDYN simulations suggest wall pumping to have a large influence on the flux of N into the core plasma, which might impede the applicability of N seeding for steady-state plasmas. Fortunately, the experimental results indicate that the simulations strongly overrate this effect. On the other hand, the common codes for power exhaust simulations are based on a similar set of assumptions, like toroidal symmetry and anomalous perpendicular transport, as the simulations presented in this work. Therefore, also simulations of N-seeded plasmas with such codes might be affected by the observed discrepancies.

Finally, we want to discuss the implications of the observed N transport on the main wall as potential contributor to the ammonia production. Analysis of the ammonia formation in low pressure plasmas indicates that the limiting physicochemical process for the NH_3 formation is the generation of nitrogen radicals in the plamsa and their hydrogenation on metallic wall surfaces [31]. Estimating the N flux to the main walls from

the N areal density at the limiter position results in a flux-density of $0.05 \cdot 10^{20}$ N/(m^{2}s). This flux-density is about a factor of 200 smaller than the N flux-density onto the outer divertor target, from where NH_3 molecules also could reach the pumping system without the need to cross the plasma. Therefore, even takting into account that the main wall surface area is roughly a factor of 10 larger than the divertor surface area, this indicates that the divertor region dominates the ammonia production. Still, it is clear that this very simplified model can only give a first idea and further analysis based on more detailed models is required.

6. Summary

The transport of N from the divertor to the outer midplane and the accumulation of N in W surfaces with varying roughness was studied in experiments at the tokamak ASDEX Upgrade. To this end samples were exposed at the outer midplane and the outer divertor to N-seeded ASDEX Upgrade plasmas and the N deposition was measured by nuclear reaction analysis. To be able to distinguish between N originating from the residual gas and injected N, the tracer isotope ^{15}N was injected into the plasma. The ^{15}N areal density on the samples exposed to the divertor plasma varies from $0.5 \cdot 10^{20}$ ^{15}N/m^2 to $3 \cdot 10^{20}$ ^{15}N/m^2. An extrapolation of these values, assuming toroidal symmetry, suggests that the ^{15}N stored in the outer divertor target accounts for 5 % of the injected atoms. The highest values are reached around the strike line, where the N deposition on the comparably rough samples has its maximum. In contrast, the N deposition on well polished bulk samples has a local minimum around the strike line. However, the similarity in the ^{15}N deposition patterns further away from the strike line indicates that the saturation

of the N areal density is rather independent of the surface morphology. Therefore, the co-deposition of N with B, whose deposition on the W coated samples also peaks in the region of the strike line, is likely to affect the N deposition on surfaces with different morphology.

The ^{15}N deposition on the tip of the sample exposed at the outer midplane is only 2–3 times smaller than the average deposition on the W coated samples exposed to the divertor plasma. Even 2 cm behind the limiters $0.1 \cdot 10^{20}$ ^{15}N/m^2 have been detected. This confirms that the main wall contributes significantly to the N storage in the plasma facing surfaces, as predicted by WallDYN. However, a quantitiative comparison to WallDYN simulations employing a model which aims to include the effect of the 3D wall structures in the 2D WallDYN simulations, predicts N areal densities which are by a factor of 4–20 higher than the ones observed in the experiment. In contrast, the N fluxes and concentrations predicted by WallDYN are lower than indicated by spectroscopic measurements in the presented discharges, with the injection of small amounts of N_2. Comparing WallDYN simulations to a set of discharges with strong N injection again shows discrepancies in the time evolution of the core N concentration. This complex picture may be due to a combination of different processes, like shortcomings in the impurity transport simulations, enhanced re-erosion of N or processes originating in the three dimensional geometry of the main wall. This suggests that further efforts aiming at an improved understanding of N re-erosion and the transport of impurities to the main wall are required for quantitative predictions.

7. Acknowledgments

This work has been carried out within the framework of the EUROfusion Consortium and has received funding from the Euratom research and training programme 2014-2018 under grant agreement No 633053. The views and opinions expressed herein do not necessarily reflect those of the European Commission.

[1] R.A. Pitts, et al., *Plasma Phys. Control. Fusion 47, B303 (2005)*, http://dx.doi.org/10.1088/0741-3335/47/12B/S22

[2] M. Bernert, et al., this conference

[3] A. Kallenbach, M. Balden, R. Dux, et al.,*J. Nucl. Mater 415, S19 (2011)*, http://dx.doi.org/10.1016/j.jnucmat.2010.11.105

[4] K. Schmid, A. Manhard et al., *Nucl. Fusion 50, 025006 (2010)*, http://dx.doi.org/10.1088/0029-5515/50/2/025006

[5] G. Meisl, K. Schmid, O. Encke, et al., *New J. Phys. 16, 093018 (2014)*, http://dx.doi.org/10.1088/1367-2630/16/9/093018

[6] D. Neuwirth, V. Rohde, T. Schwarz-Selinger, and ASDEX Upgrade Team,*Plasma Phys. Control. Fusion 54 085008 (2012)*, http://dx.doi.org/10.1088/0741-3335/54/8/085008

[7] M. Oberkofler, et al., *Phys. Scr. T167, 014077 (2016)*, http://dx.doi.org/10.1088/0031-8949/T167/1/014077

[8] L. Gao, et al., *Nucl. Fusion 56, 016004 (2015)*, http://dx.doi.org/10.1088/0029-5515/56/1/016004

[9] B.M. Berger, et al., Transient effects during erosion of WN by deuterium ions studied with the quartz crystal microbalance technique, *Nucl. Instrum. Meth. B, in press, (2016)*

[10] G. Meisl, et al., *Nucl. Fusion 56, 036014 (2016)*, http://dx.doi.org/10.1088/0029-5515/56/3/036014

[11] G. Meisl, et al., *Phys. Scr. T167, 014079 (2016)*, http://dx.doi.org/10.1088/0031-8949/T167/1/014079

[12] P. Petersson, A. Hakola, et al., *J. Nucl. Mater. 438, S616 (2013)*, http://dx.doi.org/10.1016/j.jnucmat.2013.01.129

[13] G.D. Conway, C. Angioni, et al., *Phys. Rev. Lett. 106, 065001 (2011)* , http://dx.doi.org/10.1103/PhysRevLett.106.065001

[14] G. Birkenmeier et al., *submitted to Nucl. Fus. (2016)*

[15] A. Herrmann, N. Jaksic, et al., *Fusion Eng. Des. 98, 1496 (2015)*, http://dx.doi.org/10.1016/j.fusengdes.2015.02.007

[16] G. Meisl, K. Schmid, M. Oberkofler, Nitrogen retention in ASDEX Upgrade, *J. Nucl. Mater. 463, 668 (2015)*, http://dx.doi.org/10.1016/j.jnucmat.2014.10.031

[17] C. Ruset, E. Grigore, et al., *Phys. Scr. T128, 171 (2007)*, http://dx.doi.org/10.1088/0031-8949/2007/T128/033

[18] F.B.Hagedorn and J.B.Marion, *Phys.Rev.108, 1015 (1957)*, http://dx.doi.org/10.1103/PhysRev.108.1015

[19] M. Mayer, et al., *Nucl. Instrum. Methods B143, 244 (1998)*, http://dx.doi.org/10.1016/S0168-583X(98)00383-8

[20] K. Schmid, M. Reinelt, and K. Krieger, *J. Nucl. Mater. 415, S284 (2011)*, http://dx.doi.org/10.1016/j.jnucmat.2011.01.105

[21] K. Schmid, K. Krieger, et al., *J. Nucl. Mater. 463, 66 (2015)*, http://dx.doi.org/10.1016/j.jnucmat.2014.11.109

[22] P.C. Stangeby, J.D. Elder, *J. Nucl. Mater 196, 258 (1992)*, http://dx.doi.org/10.1016/S0022-3115(06)80042-5

[23] S.W. Lisgo, A. Kukushkin, et al., *J. Nucl. Mater. 438, S580 (2013)*, http://dx.doi.org/10.1016/j.jnucmat.2013.01.121

[24] A. Hakola, M.I. Airila, et al., Global migration of impurities in tokamaks, *Plasma Phys. Control. Fusion 55, 124029 (2013)*, http://dx.doi.org/10.1088/0741-3335/55/12/124029

[25] A. Hakola, J. Karhunen, et al., *Phys. Scr. T159, 014027 (2014)*, http://dx.doi.org/10.1088/0031-8949/2014/T159/014027

[26] P.C. Stangeby, *Plasma Phys. Control. Fusion 42, B271 (2000)*, http://dx.doi.org/10.1088/0741-3335/42/12B/321

[27] U. Plank, et al., Study of the Temperature Dependent N Retention in W Surfaces by XPS, to be submitted, 2016

[28] L. Aho-Mantila, et al., *Nucl. Fusion 52, 103007 (2012)*, http://dx.doi.org/10.1088/0029-5515/52/10/103007

[29] F. Reimold, M. Wischmeier, M. Bernert, et al., *J. Nucl. Mater. 463, 128 (2015)*

[30] J. Miettunen, M.I. Airila, T. Makkonen, et al., *Plasma Phys. Control. Fusion 56, 095029 (2014)*, http://dx.doi.org/10.1088/0029-5515/52/3/032001

[31] E. Carrasco, et al., *Phys. Chem. Chem. Phys. 13, 19561 (2011)*, http://dx.doi.org/10.1039/c1cp22284h